Binary Superlattices

DOI: 10.1002/ange.201403458

Highly Ordered and Highly Aligned Two-Dimensional Binary Superlattice of a SWNT/Cylindrical-Micellar System**

*Sung-Hwan Lim, Hyung-Sik Jang, Jae-Min Ha, Tae-Hwan Kim, Pawel Kwasniewski, Theyencheri Narayanan, Kyeong Sik Jin, and Sung-Min Choi**

Abstract: *We report a highly ordered intercalated hexagonal binary superlattice of hydrophilically functionalized single-walled carbon nanotubes (p-SWNTs) and surfactant ($C_{12}E_5$) cylindrical micelles. When p-SWNTs (with a diameter slightly larger than that of the $C_{12}E_5$ cylinders) were added to the hexagonally packed $C_{12}E_5$ cylindrical-micellar system, p-SWNTs positioned themselves in such a way that the free-volume entropies for both p-SWNTs and $C_{12}E_5$ cylinders were maximized, thus resulting in the intercalated hexagonal binary superlattice. In this binary superlattice, a hexagonal array of p-SWNTs is embedded in a honeycomb lattice of $C_{12}E_5$ cylinders. The intercalated hexagonal binary superlattice can be highly aligned in one direction by an oscillatory shear field and remains aligned after the shear is removed.*

One-dimensional (1D) nanoparticles, such as single-walled carbon nanotubes (SWNTs) and metallic, semiconducting, or magnetic nanorods, have unique anisotropic physical properties suitable for a broad range of potential applications, such as optical and electronic devices,[1] sensing[2] and imaging,[3] energy storage,[4] and drug delivery.[5] The self-assembly or guided assembly of 1D nanoparticles into highly ordered superstructures with well-defined symmetry, direction, and density has been of great interest as a route to collectively enhance their physical properties and is the key to the practical realization of various potential applications. Many efforts have been made with this purpose, by the use of various methods, such as solvent evaporation,[6] external fields with patterned substrates,[7] and solution-based assembly based on various interactions.[8] Among these methods, solution-based assembly, which does not require complicated experimental setup or extensive control of evaporation conditions, has been of great interest.[8] For example, solubility control of functional groups,[9] linker-mediated interactions,[10] depletion attraction,[11] dipole–dipole[12] and electrostatic interactions,[13] and the phase behavior of amphiphilic molecules[14] have been utilized to induce the self-assembly of ordered superstructures of 1D nanoparticles, such as Au, PbSe, CdSe, CdSe/CdS nanorods, and SWNTs. However, these techniques are still in their early stages and have been focused on assemblies of single-component 1D nanoparticles.

The synthesis of binary or multicomponent superstructures of nanoparticles, which may provide new properties through synergetic coupling between different types of nanoparticles,[15] are of great interest for various potential applications as well as its own scientific merit. Exciting progress has been made in the fabrication of binary spherical-nanoparticle superlattices with various symmetries by using an interplay of entropy and van der Waals, electrostatic, and other interactions.[16] Colloidal mixtures of 1D and spherical nanoparticles have also been reported to self-assemble into three-dimensional superlattices.[17] However, systematic experimental studies on the formation of highly ordered binary superlattices by mixtures of two different types of 1D nanoparticles have been very rare, and the reported structures have been limited to simple liquid-crystalline structures, such as nematic ordering.[18] The main difficulties for the fabrication of binary 1D nanoparticle superlattices arise from the high anisotropy of the interparticle interactions and the limited availability of methods for the synthesis of highly monodisperse 1D nanoparticles with well-controlled shape and size. As the development of new and improved synthetic methods for 1D nanoparticles is progressing rapidly,[19] the latter issue has been overcome to a certain extent. However, the synthesis of highly ordered superlattices made of two different types of 1D nanoparticles still remains very challenging.

One approach to the synthesis of highly ordered binary 1D nanoparticle superlattices may be to first find conditions under which 1D nanoparticles of one type self-assemble into a highly ordered superlattice, and then to add another type of 1D nanoparticles into the preformed superlattice so that the second type of 1D nanoparticles can collectively self-assem-

[*] S.-H. Lim, Dr. H.-S. Jang, J.-M. Ha, Prof. S.-M. Choi
Department of Nuclear and Quantum Engineering
Korea Advanced Institute of Science and Technology
Daejeon, 305-701 (Republic of Korea)
E-mail: sungmin@kaist.ac.kr
Homepage: http://neutron.kaist.ac.kr
Dr. T.-H. Kim
Neutron Science Division, Department of Reactor Utilization and Development, Korea Atomic Energy Research Institute
Daejeon 305-353 (Republic of Korea)
Dr. P. Kwasniewski, Dr. T. Narayanan
European Synchrotron Radiation Facility
BP 220, 38043 Grenoble (France)
Dr. K. S. Jin
Pohang Accelerator Laboratory
University of Science and Technology
Pohang, 790-784 (Republic of Korea)

[**] This research was supported by NRF grants funded by the MEST of the Korean government (No. 2014R1A2A1A05007109 and 2011-0031931) and the KAERI grant. We acknowledge the HANARO Neutron Research Center, the PAL, and the ESRF for providing access to the beamlines used in this study. SWNT = single-walled carbon nanotube.

Supporting information for this article is available on the WWW under http://dx.doi.org/10.1002/anie.201403458.

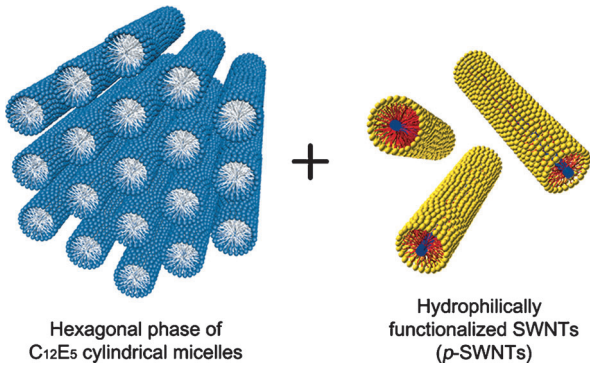

Figure 1. Mixing of two types of 1D nanoobjects. The hydrophilically functionalized SWNTs (p-SWNTs, right) are added to the cylindrical-micellar system in the hexagonal phase (left).

ble with the first type of 1D nanoparticles. In this study, we investigated how hydrophilically functionalized SWNTs, the most representative 1D nanoparticles, are self-assembled when they are added into a hexagonally packed nonionic surfactant cylindrical-micellar system (Figure 1). Small-angle X-ray and neutron scattering data showed that the binary mixture self-assembles into a highly ordered two-dimensional intercalated hexagonal binary superlattice in which a hexagonal array of functionalized SWNTs is embedded in a honeycomb lattice of cylindrical micelles. The self-assembly mechanism was considered in terms of the entropy-driven particle packing of two types of 1D nanoobjects with different diameters and the elastic-energy cost induced by the insertion of the functionalized SWNTs into the hexagonal lattice of cylindrical micelles. Although the hexagonally packed cylindrical-micellar system is not a superlattice of true 1D nanoparticles, it consists of well-defined cylinders mimicking true 1D nanoparticles and provides an excellent test bed to investigate our approach to the binary 1D-nanoparticle superlattice. The fabricated superlattice can be highly aligned in one direction by an oscillatory shear field and remains aligned after the shear is removed. To the best of our knowledge, no highly ordered and highly aligned binary superlattice of 1D nanoobjects has been demonstrated previously.

Hydrophilically functionalized SWNTs (p-SWNTs) were prepared and characterized in detail, as described elsewhere[20] (see the Supporting Information). In brief, HiPco SWNTs (2 mg mL^{-1}) and the polymerizable cationic surfactant cetyltrimethylammonium 4-vinylbenzoate (CTVB, 5 mg mL^{-1}) were mixed in D_2O and sonicated for 1 h to exfoliate bundled SWNTs. In this way, individual SWNTs were obtained with an adsorbed monolayer of CTVB. The CTVB monolayer on SWNTs was permanently fixed through in situ free-radical polymerization of the counterion (VB^-), followed by ultracentrifugation and freeze drying. The p-SWNT diameter measured by small-angle neutron scattering (SANS) was 5.0 nm, which includes the 1.0 nm diameter of isolated SWNTs and the 2.0 nm monolayer of polymerized CTVB, and the p-SWNT length measured by atomic force microscopy was approximately 500 nm. Different amounts of p-SWNTs were added to a solution of the nonionic surfactant penta(ethylene glycol) monododecyl ether ($C_{12}E_5$) in water with a fixed $C_{12}E_5$/water mixing ratio (45:55 by weight), at which the $C_{12}E_5$/water solution shows a highly ordered hexagonal phase at low temperature. For homogeneous mixing, all the mixing was carried out at temperatures at which the $C_{12}E_5$/water mixture (45:55) was in the isotropic phase. All p-SWNT/$C_{12}E_5$/D_2O samples with different amounts of p-SWNTs (0:45:55, 2:45:55, 5:45:55, 7:45:55, 10:45:55, 12:45:55, and 15:45:55) were mixed homogeneously without any visual aggregation. The UV/Vis/NIR spectra of all p-SWNT/$C_{12}E_5$/D_2O samples showed sharp van Hove transition peaks that were almost identical to those of p-SWNTs dispersed in water, thus indicating that the p-SWNTs in the mixed samples exist in an individually isolated form, as they do in water (see Figure S1 in the Supporting Information).[21]

Small-angle X-ray scattering (SAXS) measurements of the p-SWNT/$C_{12}E_5$/D_2O samples with different amounts of p-SWNTs were made as the temperature was increased from 10 to 65 °C (Figure 2 a,b; see the Supporting Information for the SAXS intensities at other mixing ratios). The $C_{12}E_5$/D_2O (45:55) mixture went through the hexagonal phase (as indicated by the peak-position ratio of $1:\sqrt{3}:2:\sqrt{7}:3$), the isotropic wormlike-micellar phase, and the lamellar phase (as indicated by the peak-position ratio of 1:2) as the temperature increased (Figure 2 a), in agreement with a previous study.[22] The SAXS intensities for the hexagonal phase are very sharp and show higher-order peaks up to the fifth order, thus indicating that the hexagonal phase is highly ordered. The diameter of $C_{12}E_5$ cylindrical micelles in the hexagonal phase was 4.44 nm, which was estimated from the lattice parameter of the hexagonal phase (6.07 nm), the density, and the concentration of $C_{12}E_5$.[23] In the lamellar phase, the lamellar spacing was 6.27 nm with a water gap of 3.23 nm.

As p-SWNTs were added to $C_{12}E_5$/D_2O (45:55), two clear changes were observed in the SAXS intensities (Figure 2 b; see also Figure S2). First, both the hexagonal-to-isotropic and the isotropic-to-lamellar phase-transition temperatures were increased. Second, in the hexagonal-phase region, new sharp peaks appeared, as indicated by arrows, and their intensities increased with the concentration of p-SWNTs. The increase in the hexagonal-to-isotropic phase-transition temperature indicates that the p-SWNTs help to maintain the hexagonal phase up to higher temperatures. Since melting of the hexagonal lattice is induced by the increased undulation of cylinders,[24] the increase in the hexagonal-to-isotropic phase-transition temperature can be attributed to the long and rigid nature of p-SWNTs. However, the p-SWNTs disturb the formation of the lamellar phase. This effect can be attributed to the fact that the diameter of p-SWNTs (5 nm) is larger than the thickness of the water layer (3.23 nm) in the lamellar phase.

The most interesting aspect of the SAXS intensities is the appearance of new sharp peaks in the hexagonal-phase region upon the addition of p-SWNTs. To understand the structures of the p-SWNT/$C_{12}E_5$/D_2O systems at low temperature, we compared the SAXS intensities of $C_{12}E_5$/D_2O (45:55) and p-SWNT/$C_{12}E_5$/D_2O (15:45:55) at 10 °C in detail (Figure 2 c). Interestingly, for p-SWNT/$C_{12}E_5$/D_2O (15:45:55), the new peak at $q = 0.736$ nm^{-1} and the peak at $q = 1.275$ nm^{-1} (which

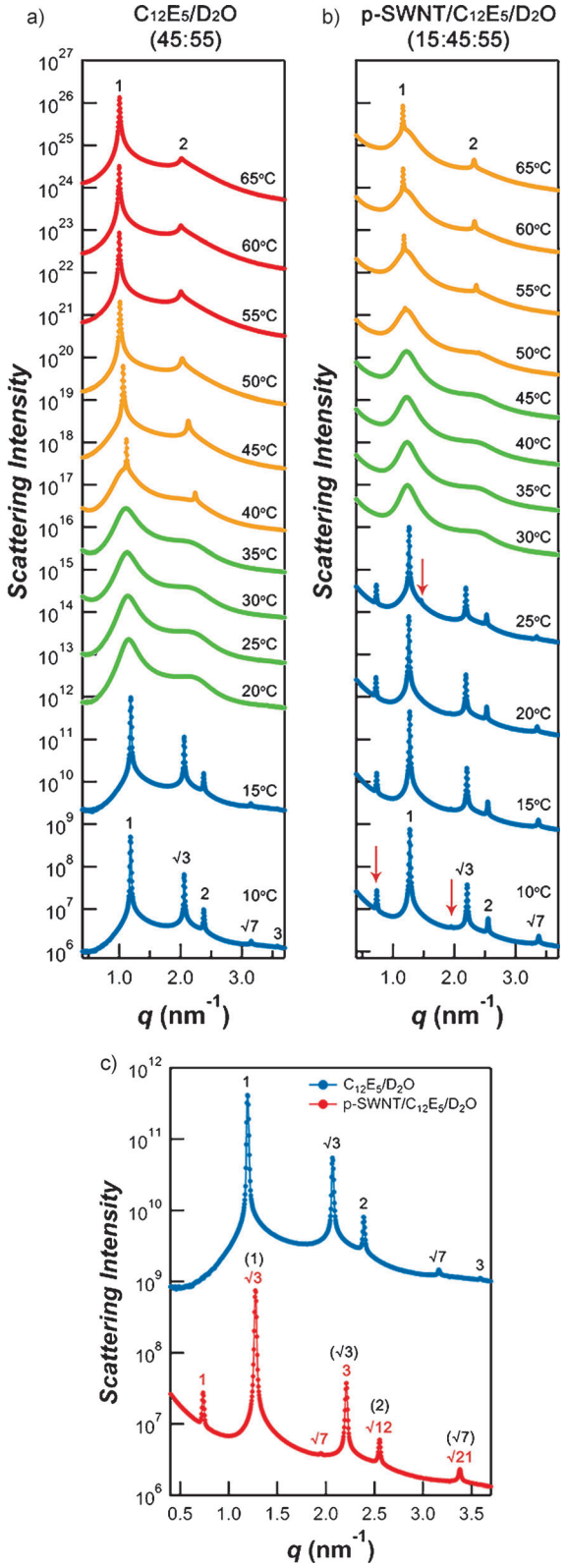

Figure 2. SAXS intensities of a) $C_{12}E_5/D_2O$ (45:55) and b) p-SWNT/$C_{12}E_5/D_2O$ (15:45:55) at different temperatures, and c) comparison of SAXS intensities of $C_{12}E_5/D_2O$ (45:55) and p-SWNT/$C_{12}E_5/D_2O$ (15:45:55) at 10°C. Scattering intensities are shifted vertically for visual clarity.

corresponds to the first-order peak of $C_{12}E_5/D_2O$ (45:55)) show a peak-position ratio of $1:\sqrt{3}$. Another new peak at $q = 1.949\ nm^{-1}$ shows a peak-position ratio of $\sqrt{7}$ with respect to the new peak at $q = 0.736\ nm^{-1}$. In fact, all the SAXS peaks of p-SWNT/$C_{12}E_5/D_2O$ (15:45:55) are directly coupled to each other with specific peak-position ratios, and can be indexed by two sets of the same peak-position ratio ($1:\sqrt{3}:2:\sqrt{7}:3:\sqrt{12}:\sqrt{21}$), as indicated by the red and black numbers in Figure 2c. This result suggests that at low temperature, p-SWNT/$C_{12}E_5/D_2O$ (15:45:55) forms a hierarchical hexagonal structure in which two hexagonal arrays are directly coupled to each other. The nearest center-to-center distance in the hexagonal arrays indicated by the peak-position ratio in red is 9.87 nm, and that in the hexagonal arrays indicated by the peak-position ratio in black is 5.70 nm. (The scattering peak positions and corresponding lattice parameters of p-SWNT/$C_{12}E_5/D_2O$ with different amounts of p-SWNTs at 10°C are summarized in the Supporting Information in Table S1 and Figure S3, respectively).

Since the new scattering peaks show up upon the addition of p-SWNTs and their intensities increase with the amount of p-SWNTs added, we expect that the new scattering peaks in the p-SWNT/$C_{12}E_5/D_2O$ (15:45:55) sample arise from correlations between p-SWNTs. To clearly confirm this hypothesis, we performed a contrast-matched small-angle neutron scattering (SANS) experiment in which the neutron-scattering length density (SLD) of water was matched with that of $C_{12}E_5$ by using a mixture of H_2O and D_2O. The SLD of p-SWNTs was adjusted by using a mixture of nondeuterated CTVB and deuterated CTVB (with fully deuterated hydrocarbon tails) for the encapsulation of SWNTs so that the contrast between p-SWNTs and the contrast-matched mixture of $C_{12}E_5$/water is enhanced (see Figure S4). In this way, only the correlation between p-SWNTs is measured.

The SANS intensities of the contrast-matched $C_{12}E_5$/water mixture (45:55) and the partially deuterated p-SWNTs mixed with contrast-matched $C_{12}E_5$/water (15:45:55) were compared with the SAXS intensity of p-SWNT/$C_{12}E_5$/water (15:45:55) (Figure 3a). The temperature was 10°C for all measurements. Whereas the SANS intensity of the contrast-matched $C_{12}E_5$/water shows essentially no correlation peaks, as expected, the SANS intensity of the partially deuterated p-SWNTs mixed with contrast-matched $C_{12}E_5$/water clearly shows two peaks. The first peak coincides with the first new peak ($q = 0.736\ nm^{-1}$) of the SAXS intensity, and the second peak coincides with the second peak ($q = 1.275\ nm^{-1}$) of the SAXS intensity, with a peak-position ratio of $1:\sqrt{3}$. This result clearly indicates that the new peaks in the SAXS intensity originate from p-SWNTs that form hexagonal arrays with a center-to-center distance of 9.87 nm and suggests that the hierarchical structures formed by p-SWNT/$C_{12}E_5$/water (15:45:55) can be represented by the illustration shown in Figure 3b. In this structure, p-SWNTs form a two-dimensional hexagonal lattice with each p-SWNT surrounded by six cylindrical micelles of $C_{12}E_5$. In other words, a hexagonal lattice of p-SWNTs is embedded in a honeycomb lattice of $C_{12}E_5$ cylinders to form an intercalated hexagonal binary superlattice.

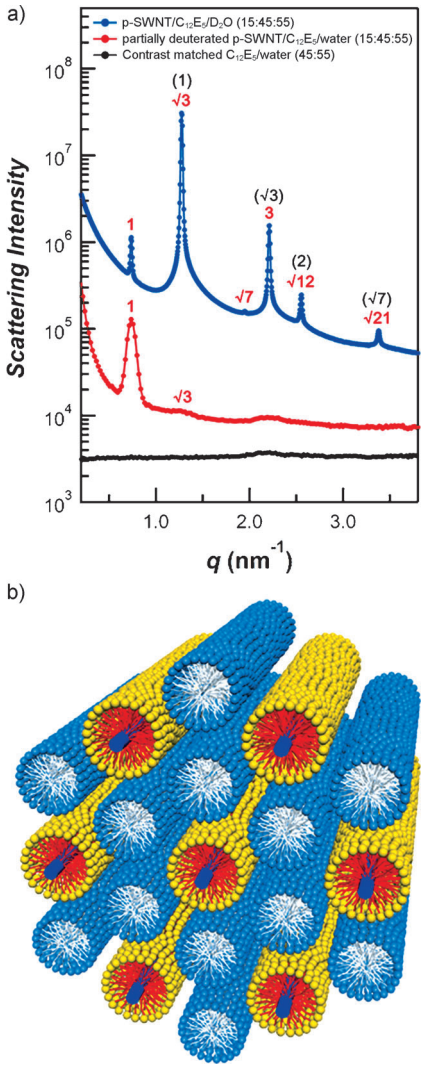

Figure 3. a) SANS intensities of contrast-matched $C_{12}E_5$/water (45:55) and partially deuterated p-SWNTs mixed with contrast-matched $C_{12}E_5$/water (15:45:55), and SAXS intensity of p-SWNT/$C_{12}E_5$/D_2O (15:45:55) at 10°C. Scattering intensities are shifted vertically for visual clarity. b) Schematic illustration of the intercalated hexagonal binary superlattice of p-SWNT/$C_{12}E_5$/water.

The SAXS and SANS measurements provide strong evidence for the proposed intercalated hexagonal binary superlattice. To unequivocally identify the structure, we carried out additional SAXS measurements for the samples under an oscillatory shear field, which aligned the intercalated hexagonal binary superlattice in one direction. For the shear experiments, the p-SWNT/$C_{12}E_5$/D_2O (10:45:55) sample was loaded in a temperature-controlled Searle-type polycarbonate shear cell with a gap of 1 mm and a wall thickness of 100 μm at the beam position.[25] The sample was slowly cooled down from the isotropic phase (ca. 30°C) to the intercalated hexagonal phase under an oscillatory shear with a shear stress of 500 Pa and a shear frequency of 5 Hz. Once the sample had cooled down well into the intercalated hexagonal phase (ca. 19°C), the shear was removed, and the 2D SAXS patterns along the radial and tangential directions were measured (Figure 4).

The 2D SAXS pattern measured along the radial direction is highly anisotropic; all the scattering peaks were found along the direction perpendicular to the flow direction (Figure 4a). The scattering peaks show a position ratio of $1:\sqrt{3}:3:\sqrt{12}$, which corresponds to the (10), (11), (30), and (22) reflections of the intercalated hexagonal binary superlattice. This result clearly indicates that the sample is unidirectionally oriented in such a way that the axes of the p-SWNTs and $C_{12}E_5$ cylindrical micelles are parallel to the flow direction. In this intercalated hexagonal binary superlattice, the (10) reflection corresponds to the first-order hexagonal peak of the p-SWNTs, and the (11) reflection corresponds to the second-order hexagonal peak of the p-SWNTs as well as the first-order peak of the $C_{12}E_5$ honeycomb lattice (inset). The azimuthally averaged scattering intensities at the (10) and (11) reflections show very sharp peaks at 90 and 270° with a full width at half maximum of 8.1 and 8.0°, respectively, thus indicating that the degree of orientation is exceptionally high.

The 2D SAXS pattern measured along the tangential direction shows clear sixfold symmetries. Each hexagonal pattern has a specific shift (30°) of the azimuthal angle relative to its neighboring hexagonal patterns (Figure 4b). This shift of the azimuthal angle between neighboring sixfold symmetries is clearly shown in the azimuthally averaged scattering intensities for the (10) and (11) reflections. These results unarguably confirm that the p-SWNT/$C_{12}E_5$/water sample indeed forms the intercalated hexagonal binary superlattice. When the intercalated hexagonal structure was aligned under the shear field, the alignment was maintained more than 24 h (see Figure S5). Although there have been many examples of highly oriented SWNT systems, most of which had no specific symmetry in the cluster of SWNTs,[1b,26] this structure is the first example of a highly oriented SWNT superstructure with hexagonal symmetry.

Such intercalated hexagonal structures have been observed in a cationic liposome–DNA complex[27] and a cationic surfactant–DNA complex[28] at isoelectric points. In these cases, the cylindrical lipid or surfactant micelles form hexagonal arrays, with each cylindrical micelle surrounded by six DNA rods (with a smaller diameter than that of the cylindrical micelles). In both cases, the self-assembly of the structure is driven by the release of counterions as cationic lipids (or cationic surfactants) and negatively charged DNA molecules compensate each other electrostatically. Since $C_{12}E_5$ is a nonionic surfactant and p-SWNT is close to neutral (or weakly positive) in charge,[11b] the formation mechanism for the intercalated hexagonal structure in the p-SWNT/$C_{12}E_5$/water system is expected to be different from that of the complexes discussed above.

The hexagonal phase of surfactant/water systems is known to be stabilized by the excluded-volume interaction between cylindrical micelles.[24a,29] The diameter of cylindrical $C_{12}E_5$ micelles in the hexagonal phase of $C_{12}E_5$/water (45:55) is 4.44 nm, and the diameter of p-SWNTs is 5 nm. Since the center-to-center distance between neighboring micelles is 6.07 nm, which results in an interstitial space of 2.57 nm in diameter, p-SWNTs cannot simply move into the interstitial space. Instead, p-SWNTs replace some of the $C_{12}E_5$ cylindrical micelles in a systematic way to form a hexagonal array

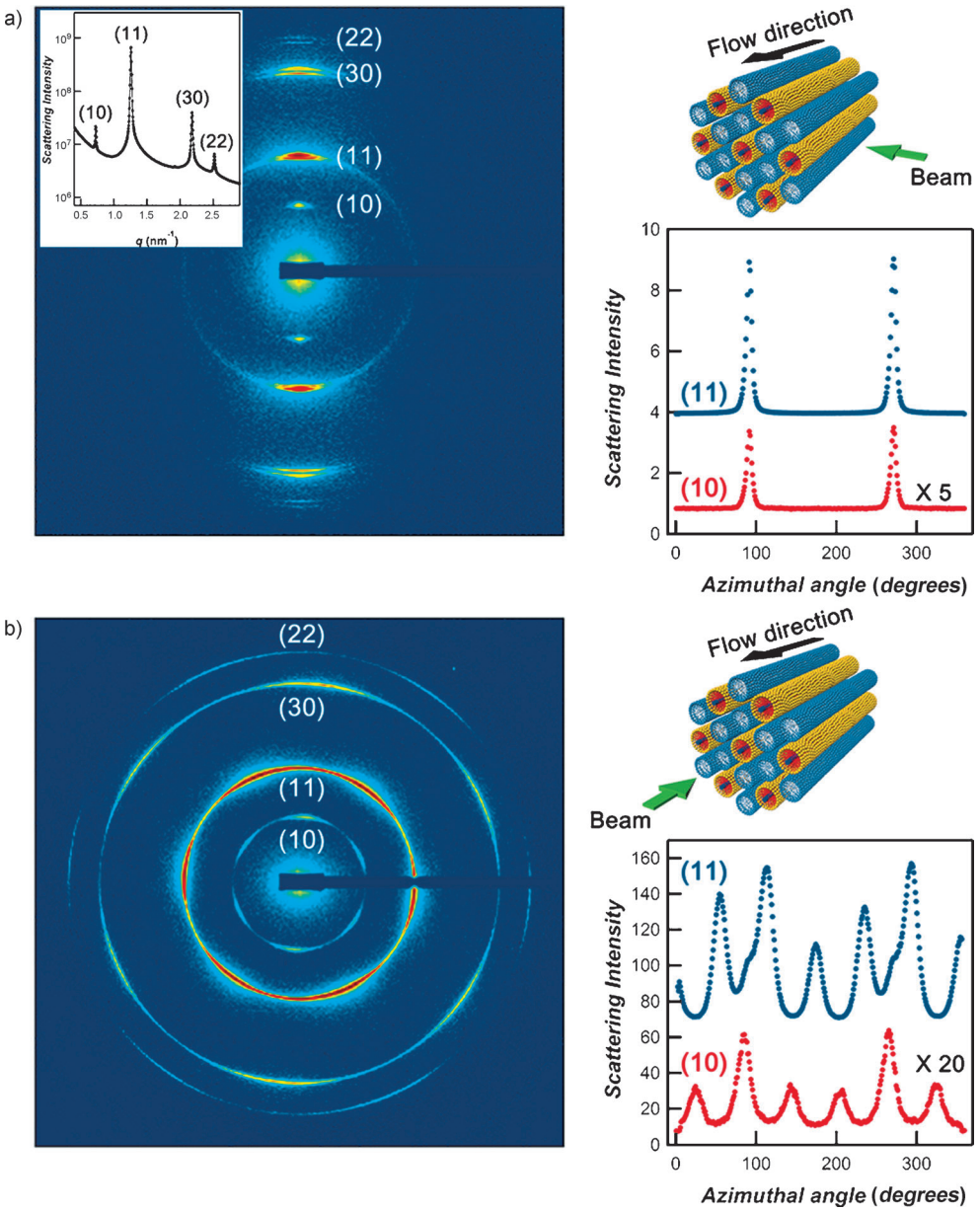

Figure 4. 2D SAXS patterns of p-SWNT/$C_{12}E_5$/D_2O (10:45:55) aligned with an oscillatory shear. The measurements were performed along a) the radial and b) the tangential beam directions. The azimuthally averaged scattering intensities along the (10) and (11) reflections are shown on the right together with the scattering geometries. The 1D SAXS intensity without shear alignment is shown in the 2D SAXS pattern of (a) as reference information.

of p-SWNTs embedded in the honeycomb lattice of $C_{12}E_5$ cylindrical micelles. In the case of binary superlattices of spherical nanoparticles with two different diameters, the entropy-driven particle packing to maximize the free-volume entropy of the particles has often been considered to be the most important factor to explain their formation mechanism, although all other interactions involved (such as electrostatic, van der Waals, and so on) need to be considered for a full understanding.[16,30] Simulations showed that AB_2- and AB_{13}-type structures of hard spheres can be driven by entropy alone, without consideration of any energetic interactions between the particles.[16a,b,31] As the observed intercalated hexagonal binary superlattice is a two-dimensional analogy of the AB_2 structure of binary spherical particles (an alternate stacking of hexagonal A planes and honeycomb B planes), the formation of the intercalated hexagonal binary superlattice may be attributed to the entropy-driven particle-packing phenomenon.[32] Whereas the configurational entropy of the binary mixture is decreased by the formation of the superlattice, the free-volume entropy of particles can be maximized by the formation of the superlattice (which provides more space for local motions of particles) and may compensate the decrease in the configurational entropy.[30–32] The formation of the intercalated hexagonal structure may be considered from the point of view of elastic distortion.[33] Since the diameter of a p-SWNT is larger than that of a $C_{12}E_5$ cylinder, p-SWNTs (which replace some of the hexagonally packed $C_{12}E_5$ cylinders) may act as impurity particles and induce the formation of stressed regions in their vicinity. The minimization of the energy cost due to the insertion of p-SWNTs may also contribute to the formation of the intercalated hexagonal superlattice. Full understanding of the superlattice formation mechanism, however, requires a more detailed theoretical investigation.

To form the intercalated hexagonal binary superlattice, the number ratio of two different cylinders should be 1:2. However, the number ratio of p-SWNT and $C_{12}E_5$ cylinders are 1:12.6, 1:9.0, 1:6.3, and 1:4.2 for the p-SWNT/$C_{12}E_5$/water samples of compositions 5:45:55, 7:45:55, 10:45:55, and 15:45:55, respectively. In this study, the number ratios were estimated from the compositions, mass densities, and diameters of p-SWNTs and $C_{12}E_5$ cylinders with the assumption that the lengths of the two types of cylinders are the same. The intercalated hexagonal binary superlattice was observed for

the sample with a number ratio as low as 1:9.0. This result may indicate that although the average number ratio is far less than 1:2, there are regions where the number ratio is close to 1:2. Possibly, p-SWNTs were not homogeneously mixed during sample preparation, or the defects formed by p-SWNTs in the hexagonal arrays of $C_{12}E_5$ cylinders (which were homogeneously distributed at the beginning) were driven to local regions, thus making the local number ratio close to 1:2. Since any experimental evidence of inhomogeneous mixing during sample preparation was not observed, however, the latter scenario may be more probable and may be understood as due to the entropy-driven attraction of p-SWNTs, which is similar to the depletion attraction in its nature. The domain sizes of the intercalated hexagonal binary superlattice as estimated from the full width at half maximum of the (10) peak (at 10 °C) by using the Scherrer equation are 137 (7:45:55), 297 (10:45:55), 332 (12:45:55), and 294 nm (15:45:55) for the samples with different compositions. The domain size in the $C_{12}E_5$/water (45:55) sample as estimated from the first-order peak (at 10 °C) is 313 nm.

In summary, we report for the first time a highly ordered intercalated hexagonal binary superlattice of p-SWNT/$C_{12}E_5$ cylindrical micelles in which a hexagonal array of p-SWNTs is embedded in a honeycomb lattice of $C_{12}E_5$ cylindrical micelles. When p-SWNTs, which have a diameter slightly larger than that of $C_{12}E_5$ cylinders, are added to the hexagonally packed $C_{12}E_5$ cylindrical-micellar system, some $C_{12}E_5$ cylinders are replaced with p-SWNTs in such a way that the free-volume entropies for both p-SWNTs and $C_{12}E_5$ cylinders are maximized, thus resulting in the intercalated hexagonal binary superlattice. The binary superlattice of the p-SWNT/$C_{12}E_5$/water system can be highly aligned in one direction by an oscillatory shear field and remains highly oriented for more than a day after the shear field is turned off. This method provides a new route for fabricating highly ordered and highly oriented SWNT superstructures. The understanding obtained in this study may provide new insight for designing methods for the synthesis of highly ordered binary superlattices of 1D nanoparticles (such as metallic, semiconducting, and magnetic nanorods, which are of great current interest) with new synergetic functionalities.

Received: March 18, 2014
Revised: August 6, 2014
Published online: September 22, 2014

Keywords: binary superlattices · one-dimensional nanoparticles · self-assembly · shear-induced alignment · single-walled carbon nanotubes

[1] a) Y. N. Xia, P. D. Yang, Y. G. Sun, Y. Y. Wu, B. Mayers, B. Gates, Y. D. Yin, F. Kim, Y. Q. Yan, *Adv. Mater.* **2003**, *15*, 353 – 389; b) M. C. LeMieux, M. Roberts, S. Barman, Y. W. Jin, J. M. Kim, Z. N. Bao, *Science* **2008**, *321*, 101 – 104.

[2] a) P. W. Barone, S. Baik, D. A. Heller, M. S. Strano, *Nat. Mater.* **2005**, *4*, 86 – 92; b) N. M. Iverson, P. W. Barone, M. Shandell, L. J. Trudel, S. Sen, F. Sen, V. Ivanov, E. Atolia, E. Farias, T. P. McNicholas, N. Reuel, N. M. A. Parry, G. N. Wogan, M. S. Strano, *Nat. Nanotechnol.* **2013**, *8*, 873 – 880.

[3] J. Choi, J. Yang, D. Bang, J. Park, J. S. Suh, Y. M. Huh, S. Haam, *Small* **2012**, *8*, 746 – 753.

[4] a) D. N. Futaba, K. Hata, T. Yamada, T. Hiraoka, Y. Hayamizu, Y. Kakudate, O. Tanaike, H. Hatori, M. Yumura, S. Iijima, *Nat. Mater.* **2006**, *5*, 987 – 994; b) H. Zhang, G. P. Cao, Z. Y. Wang, Y. S. Yang, Z. J. Shi, Z. N. Gu, *Nano Lett.* **2008**, *8*, 2664 – 2668.

[5] a) Z. Liu, K. Chen, C. Davis, S. Sherlock, Q. Z. Cao, X. Y. Chen, H. J. Dai, *Cancer Res.* **2008**, *68*, 6652 – 6660; b) Z. J. Zhang, L. M. Wang, J. Wang, X. M. Jiang, X. H. Li, Z. J. Hu, Y. H. Ji, X. C. Wu, C. Y. Chen, *Adv. Mater.* **2012**, *24*, 1418 – 1423.

[6] a) T. J. Simmons, D. Hashim, R. Vajtai, P. M. Ajayan, *J. Am. Chem. Soc.* **2007**, *129*, 10088 – 10089; b) T. Ming, X. S. Kou, H. J. Chen, T. Wang, H. L. Tam, K. W. Cheah, J. Y. Chen, J. F. Wang, *Angew. Chem. Int. Ed.* **2008**, *47*, 9685 – 9690; *Angew. Chem.* **2008**, *120*, 9831 – 9836; c) R. A. Alvarez-Puebla, A. Agarwal, P. Manna, B. P. Khanal, P. Aldeanueva-Potel, E. Carbó-Argibay, N. Pazos-Pérez, L. Vigderman, E. R. Zubarev, N. A. Kotov, L. M. Liz-Marzán, *Proc. Natl. Acad. Sci. USA* **2011**, *108*, 8157 – 8161.

[7] a) M. Chen, T. Pica, Y. B. Jiang, P. Li, K. Yano, J. P. Liu, A. K. Datye, H. Y. Fan, *J. Am. Chem. Soc.* **2007**, *129*, 6348 – 6349; b) M. S. Mauter, M. Elimelech, C. O. Osuji, *ACS Nano* **2010**, *4*, 6651 – 6658; c) C. L. Zhang, K. P. Lv, H. P. Cong, S. H. Yu, *Small* **2012**, *8*, 648 – 653.

[8] S. Y. Zhang, M. D. Regulacio, M. Y. Han, *Chem. Soc. Rev.* **2014**, *43*, 2301 – 2323.

[9] a) R. B. Grubbs, *Nat. Mater.* **2007**, *6*, 553 – 555; b) Z. H. Sun, W. H. Ni, Z. Yang, X. S. Kou, L. Li, J. F. Wang, *Small* **2008**, *4*, 1287 – 1292.

[10] a) N. Zhao, K. Liu, J. Greener, Z. H. Nie, E. Kumacheva, *Nano Lett.* **2009**, *9*, 3077 – 3081; b) Z. T. Li, Z. N. Zhu, W. J. Liu, Y. L. Zhou, B. Han, Y. Gao, Z. Y. Tang, *J. Am. Chem. Soc.* **2012**, *134*, 3322 – 3325.

[11] a) D. Baranov, A. Fiore, M. van Huis, C. Giannini, A. Falqui, U. Lafont, H. Zandbergen, M. Zanella, R. Cingolani, L. Manna, *Nano Lett.* **2010**, *10*, 743 – 749; b) C. Do, H. S. Jang, S. M. Choi, *J. Chem. Phys.* **2013**, *138*, 114701.

[12] a) K. S. Cho, D. V. Talapin, W. Gaschler, C. B. Murray, *J. Am. Chem. Soc.* **2005**, *127*, 7140 – 7147; b) D. V. Talapin, E. V. Shevchenko, C. B. Murray, A. Kornowski, S. Forster, H. Weller, *J. Am. Chem. Soc.* **2004**, *126*, 12984 – 12988.

[13] T. H. Kim, C. Do, S. H. Kang, M. J. Lee, S. H. Lim, S. M. Choi, *Soft Matter* **2012**, *8*, 9073 – 9078.

[14] a) C. Doe, H. S. Jang, T. H. Kim, S. R. Kline, S. M. Choi, *J. Am. Chem. Soc.* **2009**, *131*, 16568 – 16572; b) H. S. Jang, C. Do, T. H. Kim, S. M. Choi, *Macromolecules* **2012**, *45*, 986 – 992; c) M. S. Mauter, M. Elimelech, C. O. Osuji, *J. Am. Chem. Soc.* **2012**, *134*, 3950 – 3953; d) H. S. Jang, T. H. Kim, C. Do, M. J. Lee, S. M. Choi, *Soft Matter* **2013**, *9*, 3050 – 3056.

[15] a) J. J. Urban, D. V. Talapin, E. V. Shevchenko, C. R. Kagan, C. B. Murray, *Nat. Mater.* **2007**, *6*, 115 – 121; b) J. Chen, X. C. Ye, S. J. Oh, J. M. Kikkawa, C. R. Kagan, C. B. Murray, *ACS Nano* **2013**, *7*, 1478 – 1486.

[16] a) E. V. Shevchenko, D. V. Talapin, C. B. Murray, S. O'Brien, *J. Am. Chem. Soc.* **2006**, *128*, 3620 – 3637; b) E. V. Shevchenko, D. V. Talapin, N. A. Kotov, S. O'Brien, C. B. Murray, *Nature* **2006**, *439*, 55 – 59; c) A. Ben-Simon, H. Eshet, E. Rabani, *ACS Nano* **2013**, *7*, 978 – 986.

[17] a) Y. Nagaoka, T. Wang, J. Lynch, D. LaMontagne, Y. C. Cao, *Small* **2012**, *8*, 843 – 846; b) X. C. Ye, J. A. Millan, M. Engel, J. Chen, B. T. Diroll, S. C. Glotzer, C. B. Murray, *Nano Lett.* **2013**, *13*, 4980 – 4988.

[18] a) R. van Roij, B. Mulder, M. Dijkstra, *Physica A* **1998**, *261*, 374 – 390; b) K. R. Purdy, S. Varga, A. Galindo, G. Jackson, S. Fraden, *Phys. Rev. Lett.* **2005**, *94*, 057801; c) S. Varga, K. Purdy, A. Galindo, S. Fraden, G. Jackson, *Phys. Rev. E* **2005**, *72*, 051704; d) M. Dennison, M. Dijkstra, R. van Roij, *Phys. Rev. Lett.* **2011**, *106*, 208302; e) N. Puech, M. Dennison, C. Blanc, P. van der

Schoot, M. Dijkstra, R. van Roij, P. Poulin, E. Grelet, *Phys. Rev. Lett.* **2012**, *108*, 247801.
[19] a) A. Singh, H. Geaney, F. Laffir, K. M. Ryan, *J. Am. Chem. Soc.* **2012**, *134*, 2910 – 2913; b) X. C. Ye, L. H. Jin, H. Caglayan, J. Chen, G. Z. Xing, C. Zheng, D. N. Vicky, Y. J. Kang, N. Engheta, C. R. Kagan, C. B. Murray, *ACS Nano* **2012**, *6*, 2804 – 2817; c) X. C. Ye, C. Zheng, J. Chen, Y. Z. Gao, C. B. Murray, *Nano Lett.* **2013**, *13*, 765 – 771; d) M. L. Zhang, D. J. B. Bechstein, R. J. Wilson, S. X. Wang, *Nano Lett.* **2014**, *14*, 333 – 338.
[20] a) T. H. Kim, C. Doe, S. R. Kline, S. M. Choi, *Adv. Mater.* **2007**, *19*, 929 – 933; b) T. H. Kim, C. Doe, S. R. Kline, S. M. Choi, *Macromolecules* **2008**, *41*, 3261 – 3266; c) C. W. Doe, S. M. Choi, S. R. Kline, H. S. Jang, T. H. Kim, *Adv. Funct. Mater.* **2008**, *18*, 2685 – 2691.
[21] M. J. O'Connell, S. M. Bachilo, C. B. Huffman, V. C. Moore, M. S. Strano, E. H. Haroz, K. L. Rialon, P. J. Boul, W. H. Noon, C. Kittrell, J. P. Ma, R. H. Hauge, R. B. Weisman, R. E. Smalley, *Science* **2002**, *297*, 593 – 596.
[22] R. Strey, R. Schomacker, D. Roux, F. Nallet, U. Olsson, *J. Chem. Soc. Faraday Trans.* **1990**, *86*, 2253 – 2261.
[23] P. Lang, *J. Phys. Chem. B* **1999**, *103*, 5100 – 5105.
[24] a) J. V. Selinger, R. F. Bruinsma, *Phys. Rev. A* **1991**, *43*, 2910 – 2921; b) D. P. Bossev, S. R. Kline, J. N. Israelachvili, M. E. Paulaitis, *Langmuir* **2001**, *17*, 7728 – 7731.
[25] P. Panine, M. Gradzielski, T. Narayanan, *Rev. Sci. Instrum.* **2003**, *74*, 2451 – 2455.
[26] a) R. Haggenmueller, H. H. Gommans, A. G. Rinzler, J. E. Fischer, K. I. Winey, *Chem. Phys. Lett.* **2000**, *330*, 219 – 225; b) L. H. Lu, W. Chen, *ACS Nano* **2010**, *4*, 1042 – 1048; c) R. Allen, G. G. Fuller, Z. N. Bao, *ACS Appl. Mater. Interfaces* **2013**, *5*, 7244 – 7252; d) J. H. Olivier, P. Deria, J. Park, A. Kumbhar, M. Andrian-Albescu, M. J. Therien, *Angew. Chem. Int. Ed.* **2013**, *52*, 13080 – 13085; *Angew. Chem.* **2013**, *125*, 13318 – 13323.
[27] K. K. Ewert, H. M. Evans, A. Zidovska, N. F. Bouxsein, A. Ahmad, C. R. Safinya, *J. Am. Chem. Soc.* **2006**, *128*, 3998 – 4006.
[28] R. Krishnaswamy, V. A. Raghunathan, A. K. Sood, *Phys. Rev. E* **2004**, *69*, 031905.
[29] J. V. Selinger, R. F. Bruinsma, *Phys. Rev. A* **1991**, *43*, 2922 – 2931.
[30] Z. Chen, S. O'Brien, *ACS Nano* **2008**, *2*, 1219 – 1229.
[31] a) M. D. Eldridge, P. A. Madden, D. Frenkel, *Nature* **1993**, *365*, 35 – 37; b) X. Cottin, P. A. Monson, *J. Chem. Phys.* **1995**, *102*, 3354 – 3360.
[32] H. Xu, M. Baus, *J. Phys. Condens. Matter* **1992**, *4*, L663 – L668.
[33] Z. W. Yao, M. O. de La Cruz, *Proc. Natl. Acad. Sci. USA* **2014**, *111*, 5094 – 5099.

